Acta Materialia 256 (2023) 119107

Contents lists available at ScienceDirect

Acta Materialia

journal homepage: www.elsevier.com/locate/actamat

Full length article

Controlling solute channel formation using magnetic fields

Xianqiang Fan [a,b,*], Natalia Shevchenko [c,*], Catherine Tonry [d], Samuel J. Clark [e], Robert C. Atwood [f], Sven Eckert [c], Koulis Pericleous [d], Peter D. Lee [a,b,*], Andrew Kao [d,*]

[a] UCL Mechanical Engineering, University College London, London, WC1E 7JE, UK
[b] Research Complex at Harwell, Harwell Campus, Didcot, OX11 0FA, UK
[c] Helmholtz-Zentrum Dresden-Rossendorf, Institute of Fluid Dynamics, 01328 Dresden, Germany
[d] Computational Science and Engineering Group, University of Greenwich, London SE109LS, UK
[e] X-ray Science Division, Advanced Photon Source, Argonne National Laboratory, Lemont, IL 60439, USA
[f] Diamond Light Source Ltd, Harwell Campus, Didcot, OX11 0DE, UK

ARTICLE INFO

Keywords:
Directional solidification
Solute channel
Magnetic field
Thermoelectric magnetohydrodynamic

ABSTRACT

Solute channel formation introduces compositional and microstructural variations in a range of processes, from metallic alloy solidification, to salt fingers in ocean and water reservoir flows. Applying an external magnetic field interacts with thermoelectric currents at solid/liquid interfaces generating additional flow fields. This thermoelectric (TE) magnetohydrodynamic (TEMHD) effect can impact on solute channel formation, via a mechanism recently drawing increasing attention. To investigate this phenomenon, we combined in situ synchrotron X-ray imaging and Parallel-Cellular-Automata-Lattice-Boltzmann based numerical simulations to study the characteristics of flow and solute transport under TEMHD. Observations suggest the macroscopic TEMHD flow appearing ahead of the solidification front, coupled with the microscopic TEMHD flow arising within the mushy zone are the primary mechanisms controlling plume migration and channel bias. Two TE regimes were revealed, each with distinctive mechanisms that dominate the flow. Further, we show that grain orientation modifies solute flow through anisotropic permeability. These insights led to a proposed strategy for producing solute channel-free solidification using a time-modulated magnetic field.

1. Introduction

Gradients in temperature and composition occur in a vast range of processes, from magma flows [1,2], to salt fingers in reservoirs [3] and oceans [4,5], to industrial processes such as the solidification of nickel superalloy aeroengine turbine blades [6,7]. These variations in temperature and composition directly influence local density, hence buoyancy-driven fluid flow may occur. During metallic alloy solidification and in magma flows, preferential flow channels or chimneys are frequently observed (also termed solute finger/channels, or channel segregation), once solidified, these regions become defects, namely 'freckles' [8]. During the solidification of metallic alloys, these channels are usually formed in the interdendritic regions [9] and because they are solute-rich, they are the last to solidify and can have quite different mechanical properties from the bulk component [8,10–13]. In critical components such as single crystal superalloy turbine blades, these `freckles' can contain undesirable grain boundaries and misoriented crystals [14–16].

Both the academic and industrial communities have a strong interest in developing methods for solute channel control, including by introducing external forces to disrupt the natural convection [17–19]. An external magnetic force acting on the bulk liquid provides damping that influences mainly the uppermost mushy zone liquid. The damping effect is barely effective in the dense region of the mushy zone, due to the much lower Hartmann number, $\mathrm{Ha} = BL\sqrt{\sigma/\mu}$. The primary dendritic arm spacing is taken as the characteristic length L that is much smaller compared to that of the bulk liquid, B is the intensity of magnetic field, σ is the electrical conductivity and μ is the viscosity. During directional solidification, many other factors are at play, such as variations of temperature, solute density and Seebeck coefficient. The latter gives rise to thermoelectric currents (TECs) that are more prevalent in the mushy zone [20]. An external magnetic field can interact with the TECs and generate a Lorentz force which can change the solute flow in the mushy zone [21–24]. This phenomenon is known as thermoelectric magnetohydrodynamics (TEMHD). When properly understood, TEMHD has the

* Corresponding authors.
E-mail addresses: xianqiang.fan.19@ucl.ac.uk (X. Fan), n.shevchenko@hzdr.de (N. Shevchenko), peter.lee@ucl.ac.uk (P.D. Lee), a.kao@greenwich.ac.uk (A. Kao).

https://doi.org/10.1016/j.actamat.2023.119107
Received 14 February 2023; Received in revised form 20 June 2023; Accepted 24 June 2023
Available online 25 June 2023

potential to be an effective tool for engineers to control solute segregation [23,25,26]. This work will explore the role of the TE Lorentz force on flow dynamics, which is critical for understanding how channel segregation can be prevented. Aside from the TECs within the mushy zone, there are potentially macro-scale TECs flowing ahead of the mushy zone induced by the lateral thermal gradient resulting from the heat flux through the shell mould [7,27–29]. It is hoped a better understanding of these mechanisms will lead to the use of magnetic fields as a new process parameter to minimise freckle defects in the casting industry.

Where solute elements have significantly different X-ray absorption profiles *in situ* X-ray radiography enables us to directly observe the solute flow and dendritic evolution in real-time [30]. Great advances have been made in studying the convection during solidification using *in situ* X-ray imaging [6,18,31–33]. For instance, Reinhart et al. [6] performed *in situ* synchrotron imaging on directional solidification of a nickel-based alloy. Plume dynamics and dendritic growth were captured in their study, which are unobservable from using the traditional post-mortem characterisation. In a separate study using in situ X-ray imaging,

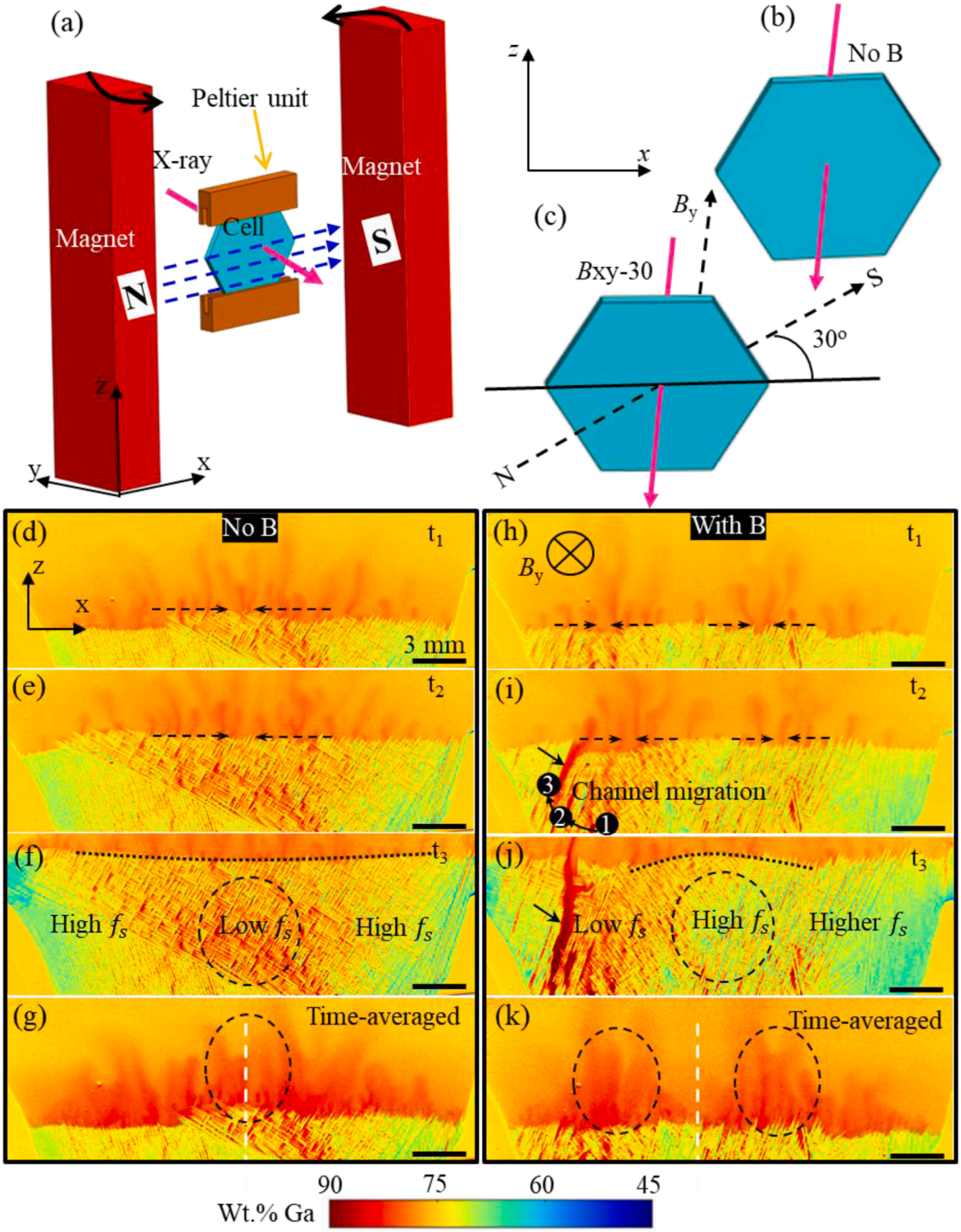

Fig. 1. Experimental setup and comparison of growing microstructure with and without magnetic field. (a) Schematic of the experimental setup. (b) Setup for the no magnet case. (c) Setup for the magnet case. The radiographs under conditions of no B at (d) t_1, (e) t_2, (f) t_3 and with B at (h) t_1, (i) t_2, (j) t_3. (g) is a time-averaged radiograph under no B condition, (k) is the time-averaged radiograph under with B condition. $t_1<t_2<t_3$. The black arrows in (i, j) indicate the solute channel.

Fautrelle et al. [34] directly observed the occurrence of channels during the solidification of an AlCu alloy in the presence of a magnetic field. Simulation has been broadly applied to predict solute channel formation and capture small-scale channel formation [35–37], but component-scale channel simulation is still a challenge.

In this study, a hexagonal Hele-Shaw cell was used to produce a convex thermal profile [32,38] creating a central solute segregation that serves as a baseline for comparison with the magnetic field case. We used *in-situ* synchrotron X-ray radiography in parallel with Cellular Automata Lattice Boltzmann-based numerical modelling [39] to study the channel segregation under the influence of a magnetic field. Ga-In alloy and Ni superalloy have similar density and the Ga-In alloy shares many other physical characteristics of Ni superalloy, in particular the solutal expansion coefficient is in the same order of magnitude (10^{-3}) for both Ga-In alloys and Ni superalloys [16,36,38]. With the lighter solute, both alloys are expected to form solute plumes, rising through the dendritic microstructure, Ga-In alloy is therefore used as a convenient analogue to Ni superalloys in this study, as it remains liquid at room temperature. A numerical model with the same sample shape and dimensions was validated by direct comparison with qualitative and quantitative analysis of the collected *in situ* data. The model, in turn, was applied to predict the flow field, which is critical for understanding the TEMHD control mechanisms. A magnetic rig was designed to provide a component of the magnetic field parallel to the X-ray, interacting with the TECs to give Lorentz forces in the plane of the thin sample radiography.

2. Methods

2.1. In situ synchrotron experimental setup

In this study, real-time observation of the directional solidification process of Ga–25wt%In alloy in the presence of a magnetic field was performed by means of synchrotron X-ray radiography. Note that Ga-25wt%In is a hypereutectic alloy. This means that during solidification, the growing dendrites are formed of the primary In phase, and Ga solute is rejected into the interdendritic liquid. As a result, less dense Ga solute plumes are formed ahead of the solidification front due to buoyancy. The solidification setup is schematically shown in Fig. 1a–c and is described in detail elsewhere [32] with only a brief outline given here. The alloy was melted and filled a hexagonal Hele-Shaw cell made of quartz. The hexagonal cell has inclined side walls, causing the isotherm shape near the edge to become convex rather than flat (Fig. 2a). The cell has an internal thickness of 200 μm and a 23 mm edge length.

A pair of independent Peltier units were mounted onto the surface at the top and bottom of the solidification cell, allowing the cooling rate and the temperature gradient to be controlled. It is important to note that the nucleation of a dendrite crystal takes place behind the bottom

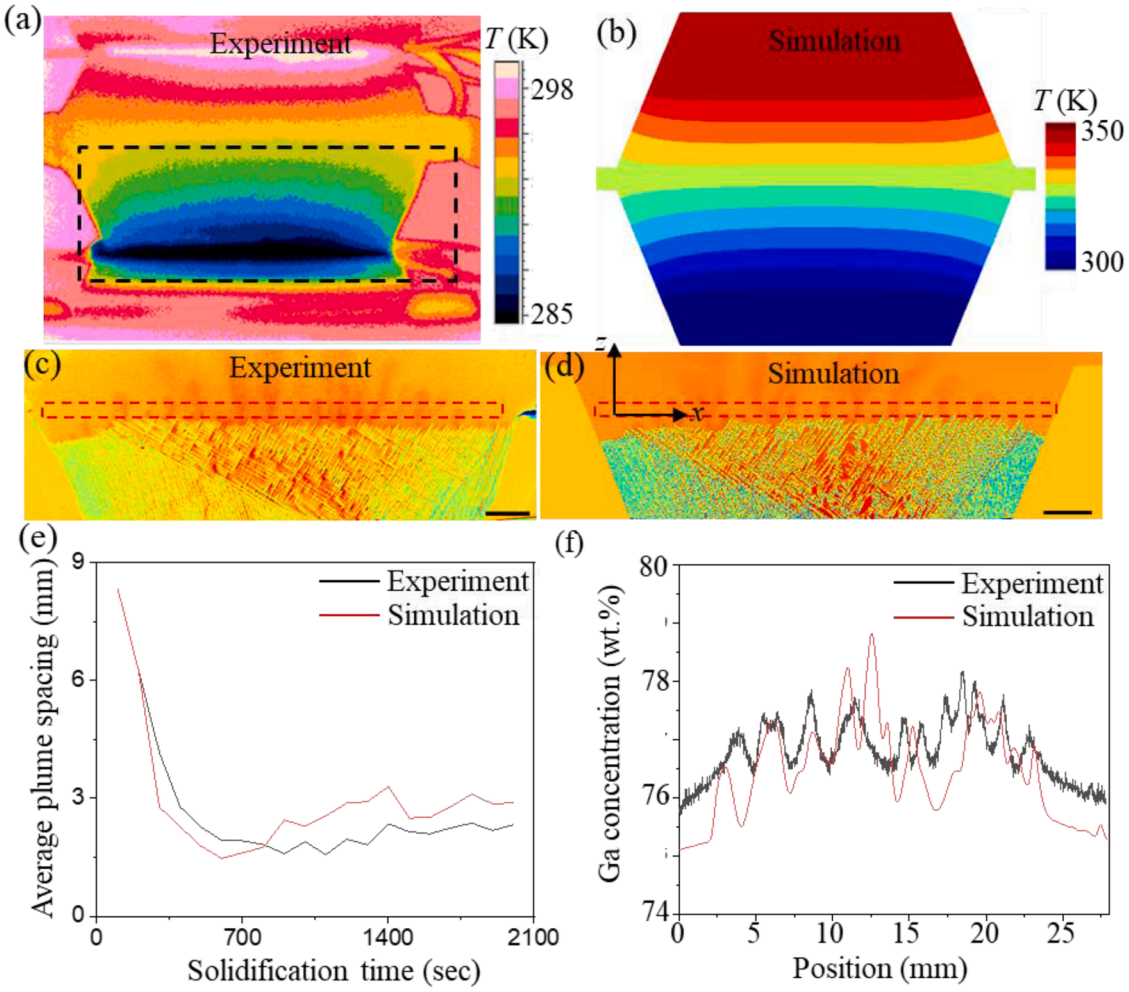

Fig. 2. Comparison between experimental results and simulation data without magnetic field. (a) Infrared image shows the sample surface temperature profile. (b) Simulation thermal profile as an initial condition. (c) Solute map extracted from radiographs. (d) Simulation predicted solute map. (e) Comparison of average plume spacing evolution between experiment and simulation. (f) Comparison of solute concentration ahead of the mushy zone between experiment and simulation, extracted from the red boxed areas in (c) and (d). The scale bars are 3 mm. (For interpretation of the references to colour in this figure legend, the reader is referred to the web version of this article.)

Peltier element. The tilt angle of the dendrite, relative to the vertical direction, is dependant on the initial growth direction of a crystal nucleus which is random and cannot be controlled in this study. Two K-type thermocouples were attached near the Peltier units to monitoring temperature. In the experiments presented, cooling rates of 0.01 K/s and 0.02 K/s and temperature gradients of 1 K/mm and 2 K/mm were applied, respectively. The solidification cell was positioned in the centre of the magnetic system composed of two permanent magnets shown in Fig. 1a. The intensity of the magnetic field in the cell position was 0.12 T at a spacing of 150 mm between the magnets. The rotation of the two magnets about a vertical cell axis allows the provision of a component of the magnetic field, perpendicular to the sample surface (B_y=0.06 T) and a component B_x= 0.10 T (Fig. 1c). The *x*-component of the magnetic field (B_x) interacts with the TECs, generating a Lorentz force in the *y* direction, perpendicular to the sample surface. However, this driving force has a minimal effect on the flow due to the thin sample thickness (200 μm).

The solidifying sample was exposed to a monochromatic, parallel X-ray beam with an X-ray photon energy of 53 keV. Conventional transmission radiographs were obtained by means of a scintillator, which was coupled to a high-speed camera (PCO. edge) with an optical module giving 18.53 μm × 18.53 μm/square pixel resolution and a field of view of 46 mm × 12 mm. Radiographs were collected at a frame rate of 5 Hz and an exposure time of 0.007 s.

A series of experiments were carried out by conducting multiple cycles of solidification and remelting. Before each experiment, the GaIn alloy was heated to a temperature of 50 °C (the melting temperature of the Ga-25wt%In alloy is approximately 25 °C) and held level for approximately 15 min to allow it to become well homogenised. After recording reference images of the completely molten alloy, the cooling of the melt and the image acquisition were initiated. Dark field images and flat field images were also recorded for further data processing. The raw images were processed to transfer pixel intensities to solute concentration using the Beer-Lambert law [40]. More information about image processing can be found in Supplementary note 1.

2.2. TESA simulation

The Thermo Electric Solidification Algorithm (TESA) is a multi-physics code developed at the University of Greenwich using a parallelised Cellular-Automata-Lattice-Boltzmann method. TESA solves the coupled equation sets for thermoelectricity, fluid flow and solidification. The computational domain comprises 4000×3200×20 cells, with each cell a cube of length 10 μm. This represents a physical domain of 40 mm x 32 mm x 200 μm encompassing the entire experimental thin sample. The hexagonal geometry is mapped onto the domain defining the region of GaIn alloy and the quartz holder. Initial conditions are applied namely, calibrated temperature field, liquid metal, homogenous composition and stagnant flow. Nucleation is assumed to take place at the base of the sample and uses either an idealised case with zero orientation and equally spaced nuclei or extrapolation of experimental data. For the latter, the time was recorded when dendrite tips first appear above the Peltier cooler. This along with the crystal orientation, was then used to extrapolate down to the base of the sample to provide nucleation data. After initialisation, transient solutions of the coupled equation set were then calculated with temporal steps of 5 ms. The detailed simulation method is in Supplementary note 2.

3. Results

3.1. Effects of magnetic field on solute transportation

Fig. 1a–c show the experimental setup. Solute transportation can be affected by the imposed magnetic field; this is observable from the radiographs in the form of plume migration and solute segregation. Plume migration appears on the interface between the mushy zone and the bulk liquid, while channel segregation takes place within the mushy zone. Both are the consequence of the flow driven by the combination of buoyancy and electromagnetic forces. During solidification, solute is rejected into the liquid forming plumes that contain high solute concentration. In the early stages of solidification, plumes thrive due to the large density contrast between solute-enriched mushy zone liquid and bulk liquid.

For the case studied, in the absence of a magnetic field plumes migrate toward the middle of the sample and the central plume is strongly pronounced in terms of its size, including both in width and height (see Fig. 1d and e and Supplementary Movie 1). Conversely, with the magnetic field applied, plumes are seen to converge and merge at two off-centre positions (see Fig. 1h and i and Supplementary Movie 2). As solidification proceeds, the mushy zone grows higher up the mould, while the bulk liquid zone diminishes and contains more solute. At this stage, unlike in the case with no magnetic field where central macro-segregation is strongest (Fig. 1f), when a magnetic field was applied with a y-component (B_y) pointing perpendicularly to the sample a solute channel appears on the left side of the sample and is not present elsewhere (Fig. 1i and j). Fig. 1g and k show the time-integrated image over the duration of the experiment by overlaying plumes onto one plane, highlighting the statistically significant change in plume distribution when applying a magnetic field. Regarding channel evolution, a channel is first initiated on the left but does not survive. Following the disappearance of the first channel, a new channel is created further to the left, this again is temporary and finally a stable channel forms even further to the left (Fig. 1i).

3.2. Influence of solute flow on microstructure

When a magnetic field is applied, the microstructure is altered. The shape of the dendrite growth front tends to be concave at the end of solidification without magnetic field as the solute accumulates in the middle and suppresses solidification, thereby there is a low solid fraction in the middle and high solid fraction at the two sides (Fig. 1f). In contrast, when applying a magnetic field, the left part of the sample clearly shows the lowest solid fraction, whereas in the middle and to the right of the sample, the solid fraction is higher (Fig. 1j). The solute-enriched plumes that spring out from the middle are suppressed, which promotes dendritic growth in the middle, whereas the plumes' merging at the two positions off the centre reduces the dendritic growth at the plume merging points, leading to a convex growth front and high solid fraction in the middle.

Counterintuitively, Fig. 1i shows that the stable channel forming region is not underneath the plumes merging position to the left, suggesting an additional force in the mushy zone has fed and stabilised this channel. Close to the left edge, the lateral thermal buoyancy is strongest due to the highest isothermal curvature, forcing the plumes to migrate to the right at a high speed while the TE Lorentz force in the mushy zone liquid transports solute to the left. This causes a mismatch between the plume meeting position to the left and the channel location. Predictions of the flow field from the simulations match those observations and will be discussed below.

3.3. Model validation

A parallel 3D model [39] simulates the entire hexagonal sample cell as the computational domain, with the capability of capturing both micro- and macro-scale phenomena. Fig. 2a shows the convex thermal profile created in the lower half of the sample by the hexagonal geometry of the cell in the experiment. The temperature variation across the lower part of the cell manifests as a cool centre and warm sides. The thermal profile applied in the simulation is convex as well, as shown in Fig. 2b. Initially the physical coordinates and orientation for each dendrite nucleus at the bottom of the sample were extrapolated from the *in situ* radiographs. Then the nuclei were seeded at the bottom of the

computational domain with the coordinates and orientations from the experiments. The model simulates the solidification process using the same conditions as in the experiments and the predicted dendrites show consistent morphology with experimental observations, as shown in Fig. 2c and d. Both the experimental and modelling results reveal central macrosegregation. The plume behaviour was also captured in the model and the average plume spacing during solidification was in good agreement with the experimental observations (Fig. 2e). Fig. 2f compares the modelled and experimentally quantified solute concentration ahead of the solidification front. Excellent agreement was achieved. This validation exercise suggests the model, which couples the physics of solidification with fluid dynamics and electromagnetics can provide a reliable interpretation of the experimental observations and potentially can then predict further phenomena.

3.4. Thermo-solutal convection without a magnetic field

With no magnetic field, solute transportation is dependant on the thermal profile and solute density variations that determine the global flow field within the sample. Fig. 3a and b show the comparison of experimental microstructure and the corresponding stage of the simulation. Though the flow is unresolvable in the experiments, the verified model can be utilised to demonstrate the flow fields. Fig. 3c and d show the predicted horizontal and vertical flow components when no magnetic field is applied. With a convex thermal profile, solute tends to accumulate at the centre of the mushy zone, as a result, solutal buoyancy is strongest at the centre where macrosegregation is observed (Fig. 3a and b) and sustained by the mushy zone feeding flow (red arrows in Fig. 3c and d). The high-speed plume induced by the central macrosegregation generates a low-pressure region in the vicinity of the interface at the centre of the sample. This causes interfacial flow from two halves of the sample pointing to the centre (pink arrows in Fig. 3c and d), leading to the plume's lateral migration (black dashed arrows in Fig. 3a and b) and intensifying the central plume. Additionally, lateral thermal buoyancy due to the convex isotherm has also contributed to the plumes' lateral migration to the centre but is only significant at the edges. Fig. 3e shows the schematic of the thermo-solutal buoyancy-driven convection. Globally, two symmetrical sample-scale flow circulations with an opposite-directional interface flow dominate the flow field in the experiment without an imposed magnetic field.

3.5. Micro/macro-scale TEMHD effects under transverse magnetic fields

With an imposed magnetic field applied, the thermally controlled convection was disrupted due to the introduction of a TE Lorentz force within the sample. Inherent TE currents (TECs) exist in the vicinity of the interface of two dissimilar materials that have distinct Seebeck coefficients during directional solidification, with the main component aligning along the thermal gradient. In this study, the TE effect creates currents on two scales. One for the micro-scale (primary) currents occurring within the mushy zone, with the dendrites and surrounding mushy zone liquid working like a thermocouple. Up-flowing TECs appear in the liquid of the mushy zone, while opposite TECs flow inside the dendrites, preserving charge conservation. The secondary macro-scale TECs occur at the interface between the bulk liquid and mushy zone (Supplementary Fig. 4). The convex isotherms with curvature changing with the mushy zone height provide both vertical and horizontal thermal gradients, which induce TECs in both directions. The primary TECs interact with the component of the external magnetic field perpendicular to the sample to generate a transverse Lorentz force within the mushy zone, transporting solute to one side. The secondary TECs are parallel to the horizontal thermal gradient and are localised to the area ahead of the mushy zone, which interacts with the y-component (B_y) of the external magnetic field to produce a vertical Lorentz force

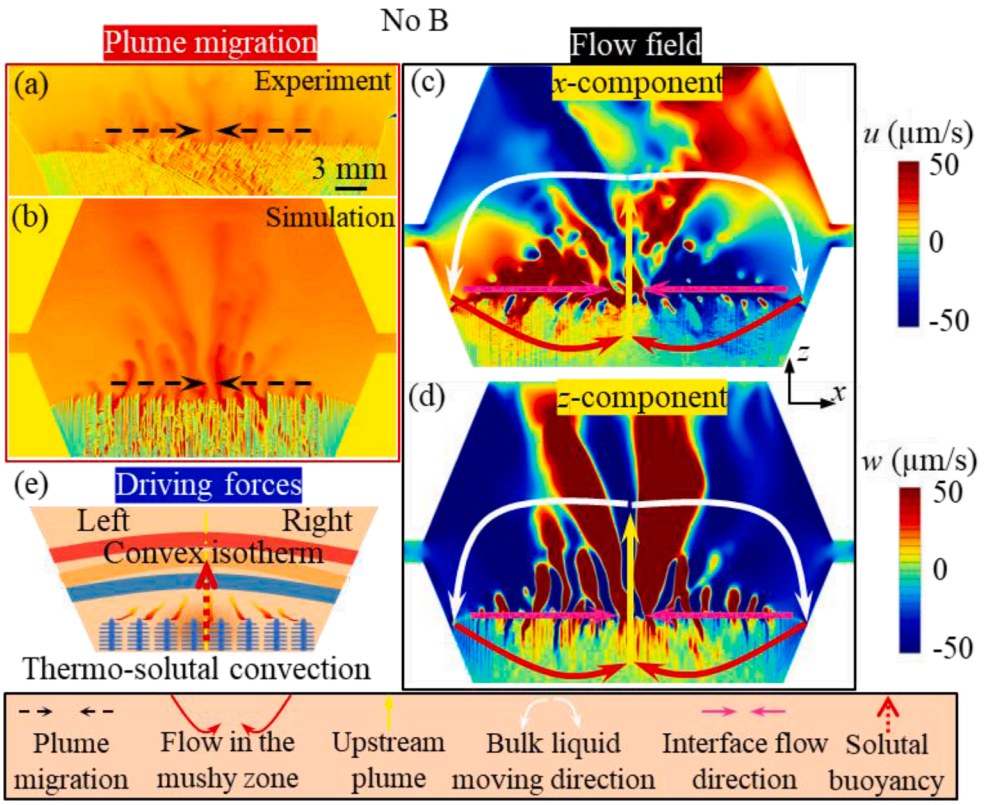

Fig. 3. Flow field without magnetic field. (a) Experimental results of microstructure without magnetic field. (b) The counterparts of modelling results of (a). The corresponding model predicted flow fields in horizontal (c) and vertical (d) directions. (e) Schematic of the driving forces that are responsible for the flow field. The legend at the bottom applies to Figs. 4 and 5 as well.

ahead of the mushy zone. Therefore, with a magnetic field applied, the flow field evolves during solidification and falls into two sequential TE regimes.

It is worth noting that the effect of TEMHD takes time to establish as the volume of fluid where the force is acting is confined to the mushy zone and becomes more important as the mushy zone grows. Further, it also takes time for macrosegregation to have a strong effect as TEMHD displaces solute. In the early stages of solidification, the plumes' behaviour shows no noticeable change compared to the no-magnetic-field case (Supplementary Fig. 5), suggesting that thermo-solutal buoyancy dominates at this stage. As solidification proceeds, the mushy zone grows and the curvature of the isotherms increases, solidification enters TE regime 1 where the plumes migrate into two off-centre positions is observed (black dashed arrows in Fig. 4a and b). In this regime, both primary and secondary TE effects are dominant and modify the migration of plumes. On the right, just off the centre, the secondary TE Lorentz force pushes liquid upwards creating a low-pressure region thus causing a new plume meeting point on the right. Though on the left the secondary TE Lorentz force is downwards, solute channel formation is dominated by a strong solutal buoyancy caused by the primary TE Lorentz force transporting solute to the left, hence there is an intensive upstream flow on the left. In the middle of the sample, the denser bulk liquid circulates downwards into the mushy zone due to gravity. From the sides of the sample, the bulk liquid is moving downwards as well to ensure mass conservation, leading to four circulations ahead of the mushy zone. Within the mushy zone, the primary TE Lorentz force continuously transports the solute to the left. Fig. 4c and d show the global flow field featuring four flow circulations ahead of the mushy zone and a lateral flow within the mushy zone, and Fig. 4e is showing the corresponding flow driving forces.

3.6. Micro-scale TEMHD dominates

Based on Bernoulli's principle, the high velocity of fluid leads to low local pressure, once macro segregation has occurred and a stable channel has formed on the left, the pressure in the vicinity of the channel opening decreases due to the high-speed fluid escaping from the channel opening, which overtakes the secondary TE effect with all plumes migrating towards the dominant channel opening instead (Fig. 5a and b). The system then switches to TE regime 2 where the plumes meeting point to the left shifts to the channel opening and the meeting point to the right vanishes. Modelling results (Fig. 5c and d) predict that there are two asymmetric flow circulations, one small circulation on the left of the channel and one large circulation on the right, feeding the channel. The interface flow is directed to the channel opening (Fig. 5c and d).

The primary TE Lorentz force acting on the inter-dendritic liquid transports solute to the left, producing a strong solutal buoyancy force on the left and initiating a channel (Fig. 5e).

This primary TEMHD effect has been further confirmed by the disappearance of channel when halving the thermal gradient despite the presence of pronounced macrosegregation on the left side of the sample (Fig. 6). The simulated plume migration across different regimes can be seen in Supplementary Movie 3 for the no magnetic field case and Supplementary Movie 4 for the magnetic field case.

3.7. Influence of grain orientation on channel formation

Aside from the driving forces (*i.e.*, buoyancy and Lorentz forces), local morphology also plays a critical role in determining channel segregation. The mushy zone liquid flows, including TE-driven horizontal flow and buoyancy-driven vertical flow, are affected by the grain orientation. The effect of orientation can be seen experimentally in Fig. 7, where three orientations, vertical, left-inclined and right-

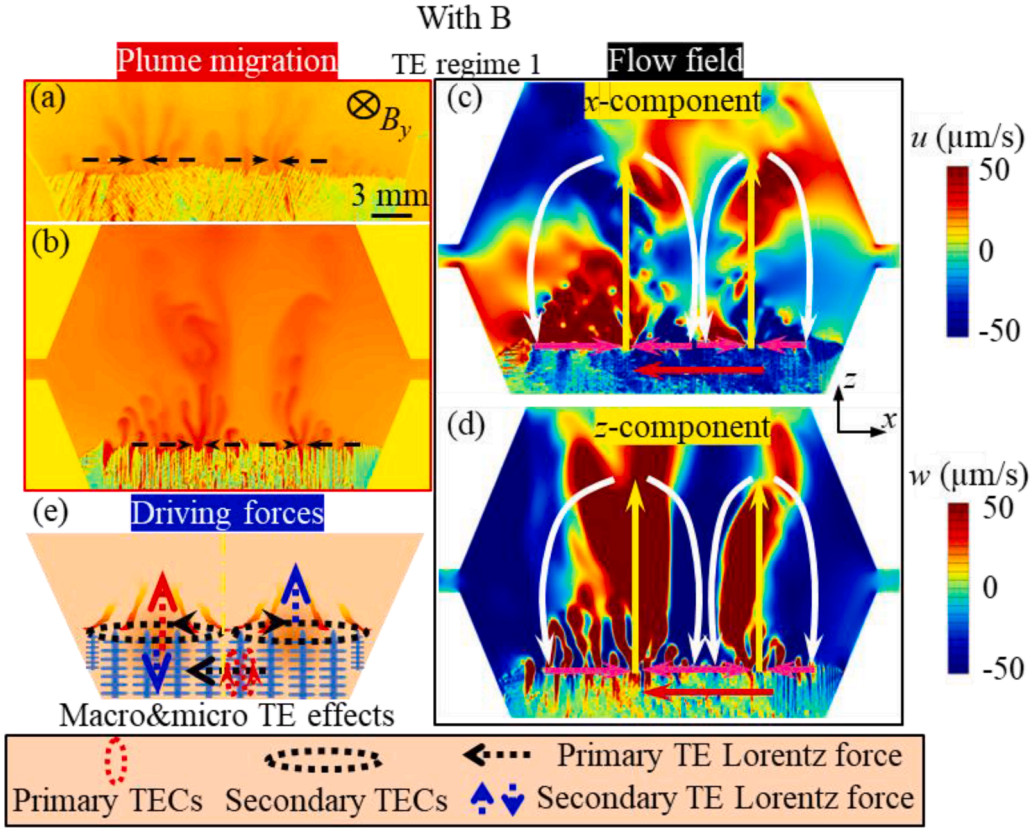

Fig. 4. Flow field with magnetic field at TE regime 1. (a) Experimental results of microstructure with magnetic field. (b) The counterparts of modelling results of (a). The corresponding model predicted flow fields in horizontal (c) and vertical (d) directions. (e) Schematic of the driving forces that are responsible for the flow field.

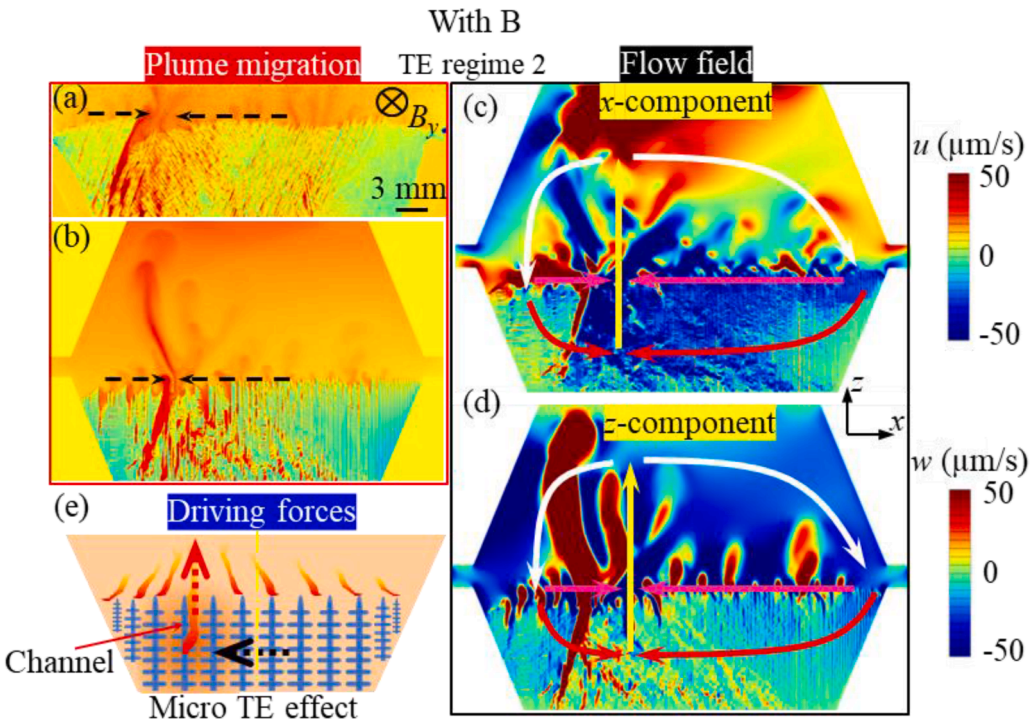

Fig. 5. Flow field with magnetic field at TE regime 2. (a) Experimental results of microstructure with magnetic field. (b) The counterparts of modelling results of (a). The corresponding model predicted flow fields in horizontal (c) and vertical (d) directions. (e) Schematic of the driving forces that are responsible for the flow field, the black arrow within the mushy zone indicates the primary TE Lorentz force.

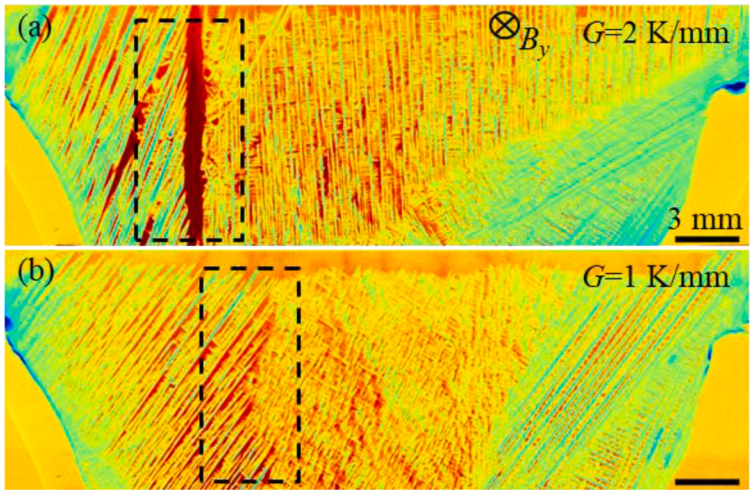

Fig. 6. Solute segregation under two thermal gradients in the presence of the magnetic field (B_y=0.03 T). (a) 2 K/mm and (b) 1 K/mm. Other processing parameters are kept consistent. Scale bars are 3 mm.

inclined, show distinctly different behaviours. Previous studies have demonstrated that the direction of grain growth can be deflected by a high magnetic field (typically >10 T) [41,42]] however, this is not the case in this study as the intensity of the applied magnetic field is two orders of magnitude lower than in those prior studies. The primary magnetic field effect that influences microstructural evolution in this study is the TE Lorentz force acting on the liquid, causing TEMHD flow.

Fig. 7a shows the channel segregation in the presence of vertical primary dendrites. Fig. 7b shows that the right-tilted dendrites cause less solute transport. Conversely, left-tilted dendrites allow the TEMHD flow to transport more solute to the left side of the sample, producing a channel in the further left position (Fig. 7c).

4. Discussion

In summary, this study reveals the TEMHD effects occurring on both macro and micro scales during directional solidification. Flow and microstructural evolution are closely intertwined. Solute transportation observed in the form of plume migration and solute segregation is controlled via the TEMHD interaction and in turn, affects the microstructure evolution. This evolving microstructure can affect the local Seebeck power, electrical conductivity, thermal profile, and permeability. Consequently, it influences the distribution of TECs and ultimately affects the TEMHD flow. A numerical model validated against experimental data was used to map the expected flow fields and microstructure development under different conditions. The evolving

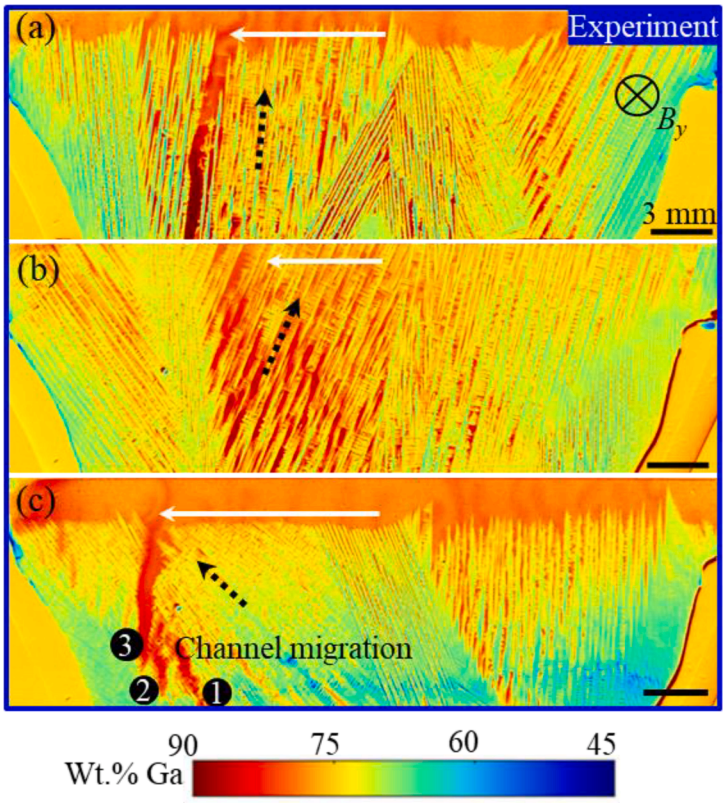

Fig. 7. Channel formation affected by the grain orientation with an imposed magnetic field. (a) Vertical grain; (b) Right-tilted grain; (c) Left-tilted grain. The white arrows measure the distance of the channel to the sample centre, the dashed black arrows indicate the grain orientation.

flow field driven by a combined Lorentz force and thermo-solutal buoyancy force is the cause of the solute segregation and plume migration. Grain orientation was found to impact the flow, with differently orientated grains leading to distinctive solute segregation patterns.

The numerical results used the same nucleation events as the validation case in Fig. 2d. To investigate the role of dendritic orientation two cases with opposite magnetic fields were run. In Fig. 8a the magnetic field direction is the same as that used in the experiments, while in Fig. 8b the magnetic field is in the opposite direction. In Fig. 8a the channel forms on the left and the grains are orientated towards the centre of the sample, while in Fig. 8b the channel forms on the right and the grains are orientated away from the centre of the sample. Due to the symmetry of the thermal profile, this provides the equivalent cases of left and right inclined in Fig. 7b and c.

In general, fluid will preferentially flow in the direction of the dominant force. In the case of horizontal flow through the dendritic network this is driven by either the thermoelectric force or horizontal pressure gradients arising to preserve continuity for a feeding flow. For vertical flow in the region where the channel forms the dominant force is solute buoyancy. However, permeability, which is a measure of how easily flow can pass through the dendritic network, plays a key role. In the case of the buoyancy driven vertical flow in the region near the mouth of the channel, dendritic growth is columnar and the permeability is anisotropic. While the dominant force is vertical, if the dendrites have a tilt away from vertical, fluid in this region will

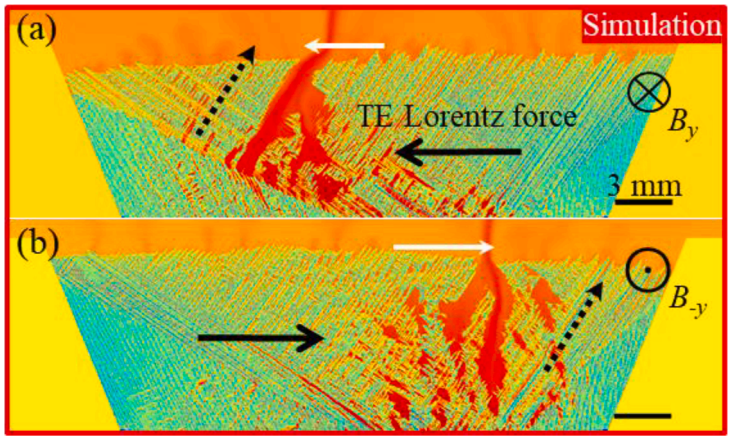

Fig. 8. Simulated channel formation with the opposite magnetic field orientations. (a) B_y directing into the page. (b) B_{-y} pointing out of the page. The white arrows indicate the distance of the channel to the sample centre, the dashed black arrows are showing the primary dendrite orientation (indicate the grain orientation).

preferentially flow along the primary dendrite arm orientation as opposed to across the dendrite arm, the path of least resistance. This has a significant impact on local thermodynamic equilibrium, depending on the direction of flow relative to the isotherms. With convex isotherms this equilibrium would take the form of convex isopleths of solute. As discussed in the previous section, the thermoelectric Lorentz force creates a bias leading to the channel formation to the left of the sample. In this region the isotherms are curved and dendrites orientated with a right tilt (Fig. 8a) will generally grow along the isotherm, resulting in flow along the isotherm. However, when the magnetic field orientation is reversed, the newly introduced TE Lorentz force points to the right, leading to the formation of a channel to the right of the sample. In this region, dendrites with a right tilt (Fig. 8b) will grow perpendicular to the isotherms along the thermal gradient, resulting in flow along the thermal gradient. To maintain thermodynamic equilibrium as fluid flows through the dendritic network, the Gibbs-Thompson condition, $\Delta T^i = m_l \Delta C^i$ should be satisfied, where T^i and C^i are the temperature and concentration at the interface, and m_l is the liquidus slope. For flow parallel to the isotherms, $\Delta T^i = 0$ and hence the concentration of the liquid is still in equilibrium. However, for flow along the thermal gradient $\Delta T^i \neq 0$ and in the case of flow escaping the interdendritic network the solute concentration in the liquid is higher than equilibrium causing remelting. This leads to a competition between the solidification front and the escaping fluid. In the case where flow is predominantly along the isotherms, the fluid cannot easily remelt the dendrites and so must escape through the interdendritic network. However, in the case where flow is along the thermal gradient, the higher concentration of solute remelts dendrites, creating a new path for solute to escape. This creates a contrasting behaviour between the two orientations, strong remelting leads to periodic slugs of solute ejected into the bulk as the channel opens. By continuity, corresponding downflow of low concentration solute causes re-solidification of the channel and the interdendritic flow finds an alternative path to melt through the dendritic network. This leads to a 'chaotic' behaviour resulting in pockets of trapped solute that can be seen experimentally in Fig. 7c and numerically in Fig. 8b. For flow parallel to the isotherms, the behaviour is more stable, with less melting and re-solidification. In the experiments a solute-enriched region formed with flow escaping through the dendritic network, being unable to melt a channel. While in the numerical results, although a channel forms, as shown in Fig. 8a it is much more stable compared to the opposite orientation in Fig. 8b (see Supplementary Movies 5 and 6).

The thermoelectric Lorentz force can be estimated by substituting characteristic values for the electrical conductivity, $\sigma = 3 \times 10^6$ S/m, Seebeck coefficient, $S = 10^{-6}$ V/K, thermal gradient, $\nabla T = 2 \times 10^3$ K/m and magnetic field $|\mathbf{B}| = 0.06$ T into $|\mathbf{J} \times \mathbf{B}| \approx \sigma S \nabla T |\mathbf{B}| = 360$ N/m^3. This value is consistent with the predictions from the numerical model. The model also predicts that the buoyancy force is similar in magnitude to the thermoelectric force *i.e.* $\rho g \beta \Delta C \approx |\mathbf{J} \times \mathbf{B}|$ and so by again taking characteristic values of density, $\rho = 6.33 \times 10^3$ kg/m^3, gravitational acceleration, $g = 9.81$ m/s^2 and solute expansion coefficient, $\beta = 1.66 \times 10^{-3}$ wt.%$^{-1}$ and substituting into the buoyancy force the concentration variation that drives buoyancy comes to $\Delta C \approx 3.4$ wt.%. This value is consistent with both predicted concentration and observed concentration variations between the mushy zone and bulk liquid and also with experimental observations. Using this value of ΔC along with a liquidus slope, $m_l = 2.9$ K/wt.%, an estimate of undercooling, $\Delta T = m_l \Delta C \approx 10$ K is obtained, reasonable for the solidification conditions. This consistency across the numerical simulations, experiment and simple estimates shows that the thermoelectric force can be as large as buoyancy and therefore significantly alter the fluid flow, hence convective transport and ultimately microstructure evolution. This finding is in agreement with the existing literature [21,43,44].

Although a thin sample was used in the experiments where the development of flow could be considerably restricted constraining dendrite growth to one plane, dendrites could still experience inclined growth in/out the page *i.e.*, zigzag growth. This would alter permeability within the mushy zone and could lead to different solute segregation compared to the vertical grain case, even though the same dendritic morphology was observed in the radiographs due to the projection nature of radiography. In addition, grain boundaries mark the interface between two adjacent grains that possess distinct primary dendrite growth directions, such as converging and diverging primary dendrite arms. The contrasting grain boundary structure has distinctive impact on solute flow and the onset of a stable solute channel, as reported by Karagadde et al. [35]. In this study due to the multi-nucleation event occurring at the bottom of the sample, grain boundaries inevitably exist that influence the flow passing through the sample, hence affecting solute segregation. Future studies will be focusing on creating a single grain in the cell *i.e.*, removing the grain boundary effect. Varying of the sample thickness is being considered to study the relationship between thickness and flow. Furthermore, based on our findings, the curvature of the liquid isotherm that is frequently encountered in casting due to the heat loss through the wall of the mould is critical in designing the flow field under an external magnetic field, hence it would be beneficial to pursue systematic studies on this in future.

The mechanism of flow control using a static magnetic field as discussed above shows that disrupting the solute flow is the key to preventing the system from initiating a stable channel. Based on our findings that applying a static magnetic field causes the channel to form on the left, periodically reversing the magnetic field would be a practical technique for mitigating freckles. Given there is a time scale for the occurrence of macrosegregation, by turning the frequency of the magnetic field reversal, we can prevent the system to becoming stable and hence a channel would not form.

5. Conclusions

By combining *in situ* synchrotron X-ray imaging and a simulation representing all the physics at play, the micro/macro TEMHD flow and its influence on solute channel formation were revealed. The studies also highlighted the role of grain orientation in modifying the solute channel formation. The major conclusions are drawn below:

1 A multiphysics model was developed coupling thermoelectricity, magnetism, fluid flow and solidification, enabling the prediction of flow and microstructural evolution under the influence of magnetic fields. This model was validated using in situ data, by comparing solute concentration, plume frequency and dendritic morphology.
2 The interplay between Lorentz force and buoyancy force drives the flow field to evolve into two regimes where different mechanisms dominate during solidification.
3 When applying a transverse magnetic field, an off-centre solute channel was formed as a result of microscopic TEMHD flow. Both experimental and simulation results show that plumes migrate to two points during the early stage of solidification, our simulation demonstrates that a macroscopic TEMHD flow is responsible for this plume lateral migration.
4 Grain orientation was found to influence solute channel formation by modifying the permeability of interdendritic flow.

Declaration of Competing Interest

The authors declare that they have no known competing financial interests or personal relationships that could have appeared to influence the work reported in this paper.

Acknowledgements

We are grateful for the use of the facilities provided by Research Complex at Harwell. We would also like to thank Diamond Light Source

for providing the beamtime (MG23423) and the staff from beamline JEEP-I12 for their technical assistance. Thank you to Peter Soar, Ivars Krastins and Sebastian Marussi for their help during the beamtime. The authors acknowledge UK-EPSRC support (grants EP/W031167/1 & EP/W032147/1), and P.D.L. support from the Royal Academy of Engineering Chair in Emerging Technologies (CiET1819/10). X.F. acknowledges the China Scholarship Council. The authors also gratefully acknowledge Dr. Joerg Grenzer (HZDR) for the ongoing scientific and experimental supports and the Department of Research Technology at HZDR for the technical support during the preparation of the experiments. S.J.C. acknowledges this research used resources of the Advanced Photon Source, a U.S. Department of Energy (DOE) Office of Science user facility at Argonne National Laboratory and is based on research supported by the U.S. DOE Office of Science-Basic Energy Sciences, under Contract No. DE-AC02–06CH11357.

Supplementary materials

Supplementary material associated with this article can be found, in the online version, at doi:10.1016/j.actamat.2023.119107.

References

[1] D. Snyder, S. Tait, Magma mixing by convective entrainment, Nature 379 (1996) 529–531, https://doi.org/10.1038/379529a0.
[2] S. Tait, K. Jahrling, C. Jaupart, The planform of compositional convection and chimney formation in a mushy layer, Nature 359 (1992) 406–408, https://doi.org/10.1038/359406a0.
[3] D.T. Burr, E.A. Sudicky, R.L. Naff, Nonreactive and reactive solute transport in three-dimensional heterogeneous porous media: mean displacement, plume spreading, and uncertainty, Water Resour. Res. 30 (1994) 791–815, https://doi.org/10.1029/93WR02946.
[4] J. Taylor, G. Veronis, Experiments on salt fingers in a Hele Shaw cell, Science (80-.) 231 (1986) 39–41, https://doi.org/10.1126/science.231.4733.39.
[5] T.J. McDougall, J.S. Turner, Influence of cross-diffusion on “finger” double-diffusive convection, Nature 299 (1982) 812–814, https://doi.org/10.1038/299812a0.
[6] G. Reinhart, D. Grange, L. Abou-Khalil, N. Mangelinck-Noël, N.T. Niane, V. Maguin, G. Guillemot, C.A. Gandin, H. Nguyen-Thi, Impact of solute flow during directional solidification of a Ni-based alloy: in-situ and real-time X-radiography, Acta Mater 194 (2020) 68–79, https://doi.org/10.1016/j.actamat.2020.04.003.
[7] N. Ren, J. Li, C. Panwisawas, M. Xia, H. Dong, J. Li, Thermal-solutal-fluid flow of channel segregation during directional solidification of single-crystal nickel-based superalloys, Acta Mater. 206 (2021), 116620, https://doi.org/10.1016/j.actamat.2020.116620.
[8] A. Hellawell, J.R. Sarazin, R.S. Steube, Channel convection in partly solidified systems, Philos. Trans. - R. Soc. London, A. 345 (1993) 507–544, https://doi.org/10.1098/rsta.1993.0143.
[9] M.G. Worster, Convection in Mushy layers, Annu. Rev. Fluid Mech. 29 (1997) 91–122, https://doi.org/10.1146/annurev.fluid.29.1.91.
[10] A.K. Sample, A. Hellawell, Mechanisms of formation and prevention of channel segregation during alloy solidification, Metall. Trans. A, Phys. Metall. Mater. Sci. 15 A (1984) 2163–2173, https://doi.org/10.1007/bf02647099.
[11] S.N. Tewari, R. Shah, Macrosegregation during dendritic arrayed growth of hypoeutectic Pb-Sn alloys: influence of primary arm spacing and mushy zone length, Metall. Mater. Trans. A Phys. Metall. Mater. Sci. 27 (1996) 1353–1362, https://doi.org/10.1007/BF02649872.
[12] M.I. Bergman, D.R. Fearn, J. Bloxham, M.C. Shannon, Convection and channel formation in solidifying Pb-Sn alloys, Metall. Mater. Trans. A Phys. Metall. Mater. Sci. 28 (1997) 859–866, https://doi.org/10.1007/s11661-997-1014-5.
[13] J.R. Sarazin, A. Hellawell, Channel formation in Pb-Sn, Pb-Sb, and Pb-Sn-Sb alloy ingots and comparison with the system NH4CI-H2O, Metall. Trans. A. 19 (1988) 1861–1871, https://doi.org/10.1007/BF02645156.
[14] M.C. Flemings, Solidification processing, Metall. Trans. 5 (1974) 2121–2134, https://doi.org/10.1007/BF02643923.
[15] B.H. Giamei, A.F. Kear, On the nature of freckles in nickel base superalloys, Metall. Trans. 3 (1970) 281–289, https://doi.org/10.4028/www.scientific.net/msf.3.281.
[16] N. Ren, C. Panwisawas, J. Li, M. Xia, H. Dong, J. Li, Solute enrichment induced dendritic fragmentation in directional solidification of nickel-based superalloys, Acta Mater. 215 (2021), 117043, https://doi.org/10.1016/j.actamat.2021.117043.
[17] S. Boden, S. Eckert, G. Gerbeth, Visualization of freckle formation induced by forced melt convection in solidifying GaIn alloys, Mater. Lett. 64 (2010) 1340–1343, https://doi.org/10.1016/j.matlet.2010.03.044.
[18] N. Shevchenko, O. Roshchupkina, O. Sokolova, S. Eckert, The effect of natural and forced melt convection on dendritic solidification in Ga-In alloys, J. Cryst. Growth. 417 (2015) 1–8, https://doi.org/10.1016/j.jcrysgro.2014.11.043.
[19] A. Noeppel, A. Ciobanas, X.D. Wang, K. Zaidat, N. Mangelinck, O. Budenkova, A. Weiss, G. Zimmermann, Y. Fautrelle, Influence of forced/natural convection on segregation during the directional solidification of Al-based binary alloys, Metall. Mater. Trans. B Process Metall. Mater. Process. Sci. 41 (2010) 193–208, https://doi.org/10.1007/s11663-009-9311-6.
[20] J.A. Shercliff, Thermoelectric magnetohydrodynamics, J. Fluid Mech. 91 (1979) 231–251, https://doi.org/10.1017/S0022112079000136.
[21] J. Wang, Y. Fautrelle, Z.M. Ren, H. Nguyen-Thi, G. Salloum Abou Jaoude, G. Reinhart, N. Mangelinck-Noël, X. Li, I. Kaldre, Thermoelectric magnetic flows in melt during directional solidification, Appl. Phys. Lett. 104 (2014), 121916, https://doi.org/10.1063/1.4870099.
[22] J. Wang, Y. Fautrelle, H. Nguyen-Thi, G. Reinhart, H. Liao, X. Li, Y. Zhong, Z. Ren, Thermoelectric magnetohydrodynamic flows and their induced change of solid–liquid interface shape in static magnetic field-assisted directional solidification, Metall. Mater. Trans. A Phys. Metall. Mater. Sci. 47 (2016) 1169–1179, https://doi.org/10.1007/s11661-015-3277-6.
[23] R. Moreau, O. Laskar, M. Tanaka, D. Camel, Thermoelectric magnetohydrodynamic effects on solidification of metallic alloys in the dendritic regime, Mater. Sci. Eng. A. 173 (1993) 93–100, https://doi.org/10.1016/0921-5093(93)90194-J.
[24] I. Kaldre, Y. Fautrelle, J. Etay, A. Bojarevics, L. Buligins, Thermoelectric current and magnetic field interaction influence on the structure of directionally solidified Sn-10 wt.%Pb alloy, J. Alloys Compd. 571 (2013) 50–55, https://doi.org/10.1016/j.jallcom.2013.03.211.
[25] A. Kao, N. Shevchenko, S. He, P.D. Lee, S. Eckert, K. Pericleous, Magnetic effects on microstructure and solute plume dynamics of directionally solidifying Ga-In alloy, Jom 72 (2020) 3645–3651, https://doi.org/10.1007/s11837-020-04305-2.
[26] X. Li, Y. Fautrelle, Z. Ren, R. Moreau, Formation mechanism of axial macrosegregation of primary phases induced by a static magnetic field during directional solidification, Sci. Rep. (2017) 1–13, https://doi.org/10.1038/srep45834.
[27] D. Szeliga, Effect of processing parameters and shape of blade on the solidification of single-crystal CMSX-4 Ni-based superalloy, Metall. Mater. Trans. B Process Metall. Mater. Process. Sci. 49 (2018) 2550–2570, https://doi.org/10.1007/s11663-018-1347-z.
[28] D. Szeliga, Reduction of freckle defect in single-crystal blade root by controlling local cooling conditions, Metall. Mater. Trans. A Phys. Metall. Mater. Sci. 53 (2022) 3224–3231, https://doi.org/10.1007/s11661-022-06752-9.
[29] D. Szeliga, K. Kubiak, J. Sieniawski, Control of liquidus isotherm shape during solidification of Ni-based superalloy of single crystal platforms, J. Mater. Process. Technol. 234 (2016) 18–26, https://doi.org/10.1016/j.jmatprotec.2016.03.003.
[30] H. Yasuda, K. Morishita, N. Nakatsuka, T. Nishimura, M. Yoshiya, A. Sugiyama, K. Uesugi, A. Takeuchi, Dendrite fragmentation induced by massive-like δ–γ transformation in Fe–C alloys, Nat. Commun. 10 (2019) 1–5, https://doi.org/10.1038/s41467-019-11079-y.
[31] N. Shevchenko, S. Eckert, S. Boden, G. Gerbeth, In situ X-ray monitoring of convection effects on segregation freckle formation, in: IOP Conf. Ser. Mater. Sci. Eng., 2012, https://doi.org/10.1088/1757-899X/33/1/012035.
[32] N. Shevchenko, S. Boden, G. Gerbeth, S. Eckert, Chimney formation in solidifying Ga-25 wt pct in alloys under the influence of thermosolutal melt convection, Metall. Mater. Trans. A Phys. Metall. Mater. Sci. 44 (2013) 3797–3808, https://doi.org/10.1007/s11661-013-1711-1.
[33] E. Liotti, C. Arteta, A. Zisserman, A. Lui, V. Lempitsky, P.S. Grant, Crystal nucleation in metallic alloys using X-ray radiography and machine learning, Sci. Adv. 4 (2018) 1–10, https://doi.org/10.1126/sciadv.aar4004.
[34] Y. Fautrelle, J. Wang, G. Salloum-Abou-Jaoude, L. Abou-Khalil, G. Reinhart, X. Li, Z.M. Ren, H. Nguyen-Thi, Thermo-electric-magnetic hydrodynamics in solidification: in situ observations and theory, Jom 70 (2018) 764–771, https://doi.org/10.1007/s11837-018-2777-4.
[35] S. Karagadde, L. Yuan, N. Shevchenko, S. Eckert, P.D. Lee, 3-D microstructural model of freckle formation validated using in situ experiments, Acta Mater. 79 (2014) 168–180, https://doi.org/10.1016/j.actamat.2014.07.002.
[36] A. Saad, C.A. Gandin, M. Bellet, N. Shevchenko, S. Eckert, Simulation of channel segregation during directional solidification of in—75 wt pct Ga. Qualitative comparison with in situ observations, Metall. Mater. Trans. A Phys. Metall. Mater. Sci. 46 (2015) 4886–4897, https://doi.org/10.1007/s11661-015-2963-8.
[37] L. Yuan, P.D. Lee, A new mechanism for freckle initiation based on microstructural level simulation, Acta Mater. 60 (2012) 4917–4926, https://doi.org/10.1016/j.actamat.2012.04.043.
[38] A. Kao, N. Shevchenko, M. Alexandrakis, I. Krastins, S. Eckert, K. Pericleous, Thermal dependence of large-scale freckle defect formation, Philos. Trans. R. Soc. A. 377 (2019), https://doi.org/10.1098/rsta.2018.0206.
[39] A. Kao, I. Krastins, M. Alexandrakis, N. Shevchenko, S. Eckert, K. Pericleous, A parallel cellular automata lattice Boltzmann method for convection-driven solidification, Jom 71 (2019) 48–58, https://doi.org/10.1007/s11837-018-3195-3.
[40] W.U. Mirihanage, K.V. Falch, I. Snigireva, A. Snigirev, Y.J. Li, L. Arnberg, Retrieval of three-dimensional spatial information from fast in situ two-dimensional synchrotron radiography of solidification microstructure evolution, Acta Mater. 81 (2014) 241–247, https://doi.org/10.1016/j.actamat.2014.08.016.
[41] X. Li, Y. Fautrelle, Z. Ren, Morphological instability of cell and dendrite during directional solidification under a high magnetic field, Acta Mater. 56 (2008) 3146–3161, https://doi.org/10.1016/j.actamat.2008.03.018.

[42] X. Li, Y. Fautrelle, Z. Ren, Influence of a high magnetic field on columnar dendrite growth during directional solidification, Acta Mater. 55 (2007) 5333–5347, https://doi.org/10.1016/j.actamat.2007.05.036.
[43] X. Li, Y. Fautrelle, A. Gagnoud, D. Du, J. Wang, Z. Ren, H. Nguyen-Thi, N. Mangelinck-Noel, Effect of a weak transverse magnetic field on solidification structure during directional solidification, Acta Mater. 64 (2014) 367–381, https://doi.org/10.1016/j.actamat.2013.10.050.
[44] X. Li, A. Gagnoud, Z. Ren, Y. Fautrelle, R. Moreau, Investigation of thermoelectric magnetic convection and its effect on solidification structure during directional solidification under a low axial magnetic field, Acta Mater. 57 (2009) 2180–2197, https://doi.org/10.1016/j.actamat.2009.01.016.